Measurement of the tau anomalous magnetic moment

L. Taylor[a*]

[a]Department of Physics, Northeastern University, Boston, MA 02115, U.S.A.

We have analysed radiative $e^+e^- \to \tau\tau(\gamma)$ events using $84\,\mathrm{pb}^{-1}$ of data collected by the L3 experiment during the 1992-1994 LEP runs at the Z resonance. The energy spectrum of the photons is compared to the predictions of QED including additional magnetic and electric dipole terms. No deviations from the standard model are observed so upper limits are set on the magnetic and electric dipole form factors of the tau.

1. INTRODUCTION

In the standard model, the electromagnetic interactions of each of the three charged leptons are assumed to be identical, apart from mass effects. There is, however, no experimentally verified explanation for why there are three generations of leptons nor for why they have such differing masses. New insight might be forthcoming if the leptons were observed to have substructure which could manifest itself experimentally in anamalous values for the magnetic or electric dipole moments. The anomalous moments for the electron and muon are already severely constrained[1]. The tau is of particular interest since it is relatively poorly measured and, being the heaviest lepton, it may be the most sensitive to new physics.

We analyse data collected by the L3 detector at LEP during 1992–1994, corresponding to an integrated luminosity of $84\,\mathrm{pb}^{-1}$. We study the couplings of the photon to the tau using the energy spectrum of photons radiated in $\tau\tau$ events produced in e^+e^- collisions at $\sqrt{s} \approx m_Z$. From a fit to the photon energy spectrum, allowing for standard model backgrounds, we derive constraints on the anomalous magnetic moment and the electric dipole moment of the tau.

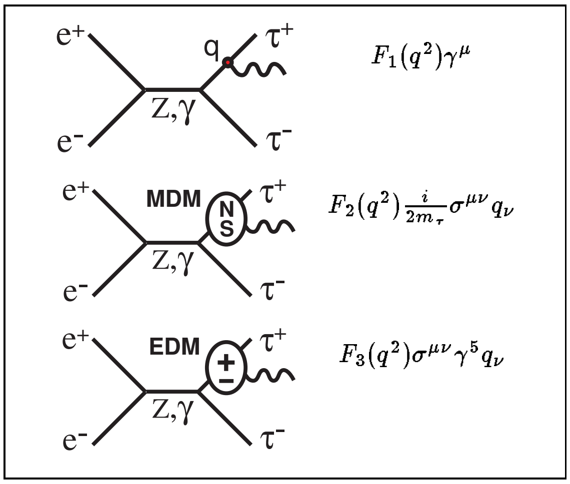

Figure 1. Photon couplings to a tau produced in an e^+e^- collision, induced by an electric charge (top), a magnetic dipole moment (centre), or an electric dipole moment (bottom).

2. ANOMALOUS DIPOLE MOMENTS

In general a photon may couple to a tau through its electric charge, magnetic dipole moment, or electric dipole moment (neglecting possible anapole moments[2]), as shown schematically in figure 1 for taus produced in e^+e^- collisions. The most general Lorentz-invariant form of the coupling of a tau to a photon of 4-momentum q_ν is obtained by replacing the usual γ^μ by

$$\begin{aligned}\Gamma^\mu &= F_1(q^2)\gamma^\mu \\ &+ F_2(q^2)\frac{i}{2m_\tau}\sigma^{\mu\nu}q_\nu - F_3(q^2)\sigma^{\mu\nu}\gamma^5 q_\nu. \quad (1)\end{aligned}$$

*Representing the L3 Collaboration

The q^2-dependent form-factors, $F_i(q^2)$, have familiar interpretations for $q^2 = 0$: $F_1(q^2=0) \equiv q_\tau$ is the electric charge of the tau; $F_2(q^2 = 0) \equiv a_\tau = (g-2)/2$ is the static anomalous magnetic moment of the tau (where g is the gyromagnetic ratio); $F_3(q^2=0) \equiv d_\tau/q_\tau$, where d_τ is the static electric dipole moment of the tau.

In the standard model, a_τ is non-zero due to loop effects. It has been calculated to be[3]

$$a_\tau = \alpha/2\pi + \ldots = 0.001\,177\,3(3). \tag{2}$$

A non-zero value of d_τ is forbidden by both P invariance and T invariance. Assuming CPT invariance, observation of a non-zero value of d_τ would imply CP violation in the τ system.

In order to parametrise the effects of an anomalous magnetic moment on photon production in $e^+e^- \to \tau^+\tau^-$ events, the substitution:

$$\gamma^\mu \longrightarrow \gamma^\mu + i\frac{F_2(q^2)}{2m_\tau}\sigma^{\mu\nu}q_\nu \tag{3}$$

is made at the $\tau\tau\gamma$ vertex. Similarly for electric dipole moments we substitute:

$$\gamma^\mu \longrightarrow \gamma^\mu + F_3(q^2)\sigma^{\mu\nu}\gamma^5 q_\nu. \tag{4}$$

We do not consider the effects of F_2 and F_3 simultaneously. The effects of the extra terms on the number of photons radiated, N_γ, are then *assumed* to factorise into a standard model contribution and an anomalous contribution, *i.e.*

$$\frac{dN_\gamma}{dE_\gamma d\xi_{\gamma\tau}} = \frac{dN_\gamma^{\mathrm{SM}}}{dE_\gamma d\xi_{\gamma\tau}} + \frac{dN'_\gamma(F_2)}{dE_\gamma d\xi_{\gamma\tau}}, \tag{5}$$

where E_γ denotes the photon energy and $\xi_{\gamma\tau}$ denotes the angle between the photon and the τ^+, both measured in the laboratory frame. This approximation neglects terms linear in F_2, which scale with $\mathrm{m}_\tau^2/\mathrm{m}_\mathrm{Z}^2$, and interference of initial and final state radiation. The validity of these approximations is discussed in section 4.

Within this model, the calculations for the electric dipole moment are equivalent to those for the anomalous magnetic moment, given the substitution: $F_2/2m_\tau \longrightarrow F_3$. We therefore describe the analysis in terms of F_2 and ultimately trivially convert the constraints obtained on F_2 to constraints on F_3.

The effect of the anomalous term is to enhance the production of photons, particularly at high energies. Integrating over $\xi_{\tau\gamma}$, we obtain for the full 4π acceptance:

$$\frac{dN'}{dE_\gamma} = 4F_2^2 E_\gamma \frac{\Gamma_\mathrm{e}}{\Gamma_\mathrm{Z}^2}\frac{\mathcal{L}\alpha^2}{m_\mathrm{Z} m_\tau^2 \sin^2\theta_\mathrm{W}\cos^2\theta_\mathrm{W}} \times \frac{1}{4}\left(\frac{2}{3}g_\mathrm{A}^2\frac{E_\gamma^2}{m_\mathrm{Z}^2} + (g_\mathrm{V}^2 + g_\mathrm{A}^2)\left(1 - 2\frac{E_\gamma}{m_\mathrm{Z}}\right)\right) \tag{6}$$

where: $\mathcal{L}$ is the integrated luminosity; α is the electromagnetic coupling constant; m_Z and Γ_Z are the Z mass and width; Γ_e is the electronic partial width of the Z; m_τ is the tau mass; θ_W is the weak mixing angle; and $g_\mathrm{V} \approx -0.0376$ and $g_\mathrm{A} \approx -0.5008$ are the vector and axial-vector coupling strengths.

Figure 2 shows the differential energy distribution of anomalous photons, assuming the same integrated luminosity as used in this analysis, for anomalous magnetic moments of $F_2 = 0.02$, 0.04, and 0.06 which span the sensitivity of the data. The numbers of events expected for these values are 21, 82, and 185 respectively assuming full acceptance and 100% efficiency. Note the enhancement at high energies compared to the rapidly falling spectrum of standard model initial and final state radiation.

3. L3 ANALYSIS OF $\tau\tau\gamma$ EVENTS

This analysis is based on data collected by the L3 experiment during the 1992–1994 LEP runs. We use only events taken on the Z peak corresponding to an integrated luminosity of $84\,\mathrm{pb}^{-1}$.

3.1. The L3 detector

The L3 detector, shown in figure 3, is described in detail elsewhere[4,5]. The central tracking chamber is a Time Expansion Chamber (TEC) consisting of two coaxial cylindrical drift chambers with 12 inner and 24 outer sectors. The Z-chamber surrounding the TEC consists of two coaxial proportional chambers with cathode strip readout. The electromagnetic calorimeter is composed of bismuth germanate (BGO) crystals. The energy resolution of the BGO for photons above $3.5\,GeV$, as selected in this analysis, is approximately 1.4%. Hadronic energy depositions are

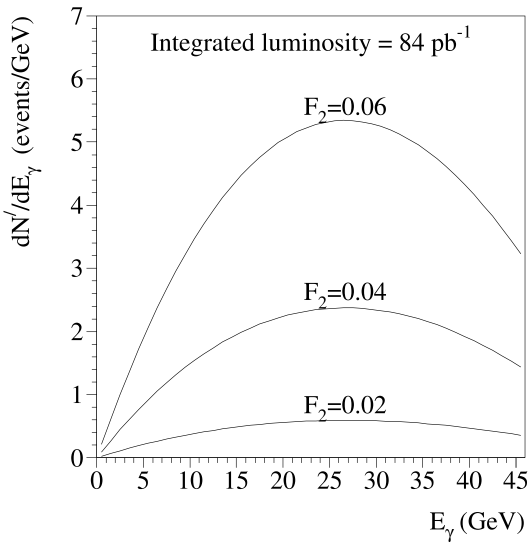

Figure 2. Energy spectrum of anomalous photons for $F_2 = 0.02, 0.04, 0.06$.

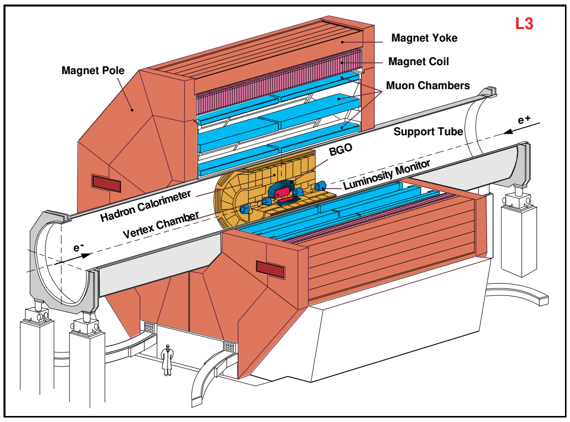

Figure 3. Perspective view of the L3 detector.

measured by a uranium proportional wire chamber sampling calorimeter surrounding the BGO. Scintillator time-of-flight counters are located between the electromagnetic and hadronic calorimeters. The muon spectrometer, located outside the hadron calorimeter, consists of three layers of drift chambers measuring the muon trajectory in both the bending and the non-bending planes. All subdetectors are installed inside a solenoidal magnet which provides a uniform field of 0.5 T.

3.2. Selection of $\tau\tau(\gamma)$ events

The selection of $\tau\tau(\gamma)$ events is restricted to barrel region, *i.e.* $|\cos\theta_{\mathrm{thrust}}| < 0.73$ where θ_{thrust} is the thrust axis of the event. The main cuts used for rejecting non-$\tau\tau$ events are described below. Hadronic events are rejected by requiring the event to have small numbers of charged tracks and energy clusters. Two photon events are rejected by requiring that the event contains two jets, one with $E > 6GeV$ and the other with $E > 2GeV$. No acollinearity cut is applied since this would preferentially reject $\tau\tau$ events containing a high energy photon. Di-muon events are rejected by requiring that there be no muon track in the muon spectrometer with momentum greater than $42GeV$, nor any muon track opposite a minimum-ionising signal in the calorimeters. To reject Bhabha events we require that there be no bumps in the BGO with energy greater than $40GeV$, unless the bump has been identified as a photon. Radiative Bhabha events are rejected by requiring that the total energy recorded in the BGO is less than $78GeV$.

A sample of 66 218 candidate $\tau\tau(\gamma)$ events survive these cuts. Figure 4 shows a typical $\tau\tau(\gamma)$ candidate event. The decay products of the taus in this event leave tracks in the Time Expansion Chamber (TEC) and energy in the BGO and hadron calorimeters. The photon has no associated track, leaves a considerable amount of energy in the BGO, and no energy in the hadron calorimeter. In addition to its distinctive signature, the photon is also well isolated from the decay products of the taus.

To study the selection of $\tau\tau(\gamma)$ events we use simulated events generated with the KORALZ Monte Carlo program[6], which in turn uses TAUOLA[7] for τ decays and PHOTOS[8] for (multiple) standard model photon radiation. The simulated events are passed through the GEANT-

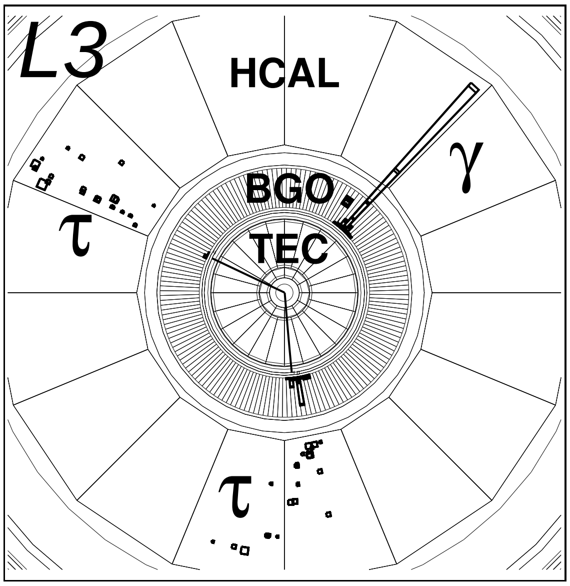

Figure 4. Typical $\tau\tau\gamma$ candidate event.

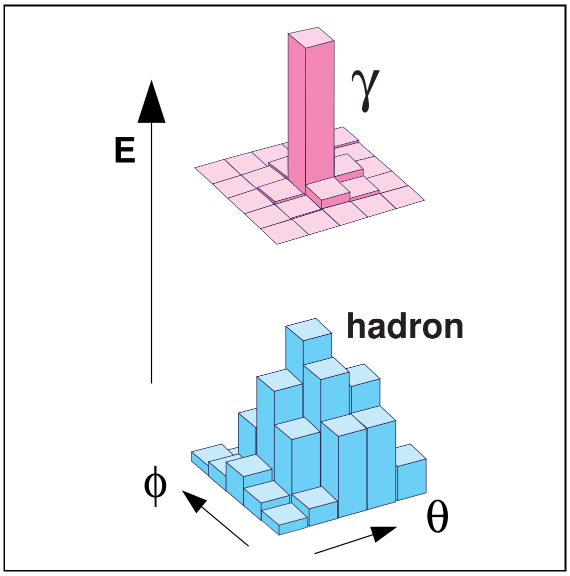

Figure 5. Shower shapes in the BGO.

based L3 detector simulation program[9] which allows for the effects of energy loss, multiple scattering, interactions and decays in the detector material as well as time-dependent detector effects. These events are then reconstructed using the same algorithms as for the data.

The background of non-$\tau\tau(\gamma)$ events is estimated from the simulated event sample to be $3.2 \pm 0.5\%$. The $\tau\tau(\gamma)$ efficiency in the fiducial volume is $83.4 \pm 0.1\%$ which corresponds to an efficiency of $51.5 \pm 0.1\%$ for the full solid angle. As a cross-check, these quantities and their errors were used to evaluate the peak $\tau\tau(\gamma)$ cross-section at $\sqrt{s} \approx m_Z$. The result obtained is $\sigma_{\tau\tau} = 1.483 \pm 0.015\,\mathrm{nb}$, which is in good agreement with the ZFITTER[10] prediction of $\sigma_{\tau\tau} = 1.48\,\mathrm{nb}$.

3.3. Selection of photons in $\tau\tau(\gamma)$ events

Photon candidates are identified by a shower in the BGO with no associated track in TEC and no energy in the neighbouring region of the hadron calorimeter. The transverse profile of electromagnetic showers in the BGO is considerably narrower than for hadronic showers, as shown in figure 5. Photon candidates are therefore required to have a narrow shower profile which is statistically consistent with that of an electromagnetic shower.

Figure 6 shows the polar angle distribution of photon candidates selected in the Monte Carlo sample. The large bump in the central region reflects the requirement that the event thrust is in the BGO barrel region. There is a considerable background at small angles with respect to the beam due to initial state radiation (ISR)[2]. Photon candidates are therefore required to be in the BGO barrel only, corresponding to $|\cos\theta| < 0.7$ where θ is the polar angle with respect to the beam.

After applying these selection criteria, the sample of photon candidates consists of genuine photons from initial and final state radiation and

[2]The KORALZ treatment of photon radiation permits photons to be tagged as initial or final state, although these are of course indistinguishable both theoretically and experimentally.

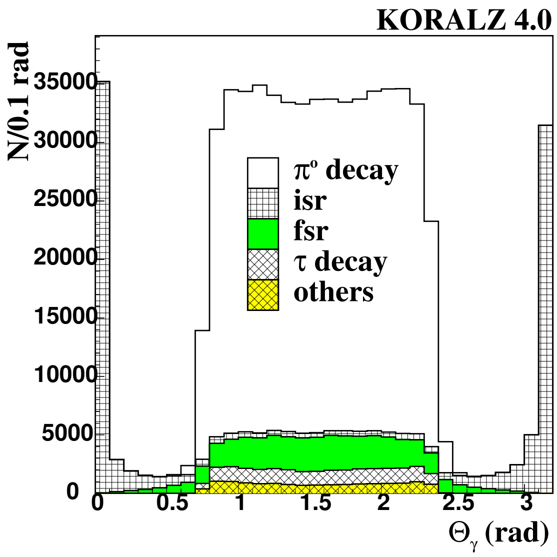

Figure 6. Polar angle distribution of preselected photon candidates in $\tau\tau(\gamma)$ events.

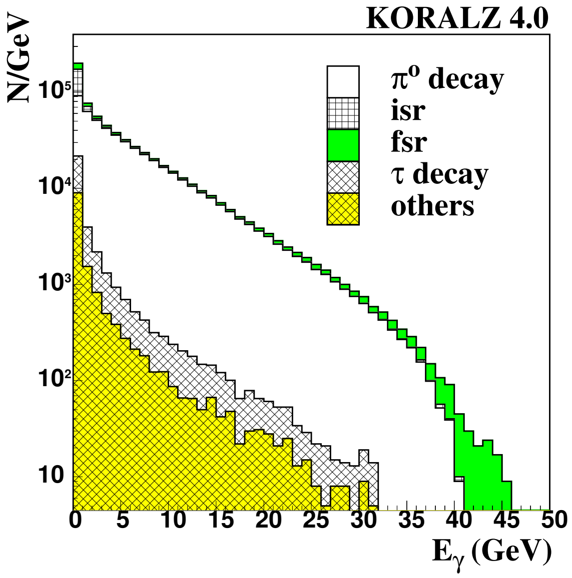

Figure 7. Energy spectrum of photon candidates prior to the energy and isolation cuts, for the KORALZ simulated event sample.

from $\pi^0 \to \gamma\gamma$ decays, with a small contribution from mis-identified decay products of the tau.

Figures 7 and 8 show the distributions of the photon energy and the isolation angle between the photon candidate and the closest tau jet, as determined from the KORALZ Monte Carlo sample. Since the contribution to the energy spectrum due to anomalous tau moments is peaked at high energies, as shown in figure 2, the energy of photon candidates is required to be greater than $3.5\,GeV$. These photons also tend to be isolated so, to reduce backgrounds, the isolation angle is required to be greater than 280 mrad.

After application of these cuts, the standard model background consists of initial and final state radiation photons with a small $(0.4 \pm 0.1)\%$ contribution of photons from π^0 decays.

3.4. Results

To determine F_2, or equivalently F_3, a maximum likelihood fit is made to the measured photon energy spectrum. The standard model background contribution is estimated from the fully simulated KORALZ Monte Carlo event sample, weighted according to the integrated luminosity of the data. The additional contribution, assuming an ideal detector, is given by equation 6. This expression is reweighted to allow for: the $\tau\tau(\gamma)$ event selection efficiency, which is studied using radiative photons in KORALZ events; the polar angular acceptance for photons; and the phase space acceptance for photons (*i.e.* the photon energy cut). The only free parameter in the fit is $F_2^2(0)$. This is more appropriate than $F_2(0)$ since the number of additional events expected scales with $F_2^2(0)$. The inclusion of anomalous moments affects both the shape and the normalisation of the photon spectrum. For this analysis, these contribute approximately equally to the sensitivity. [3]

[3] It is worth noting that the so-called Extended Maximum Likelihood method, which enforces the normalisation of the data and the hypothesis, will tend to yield an artificially good limit.

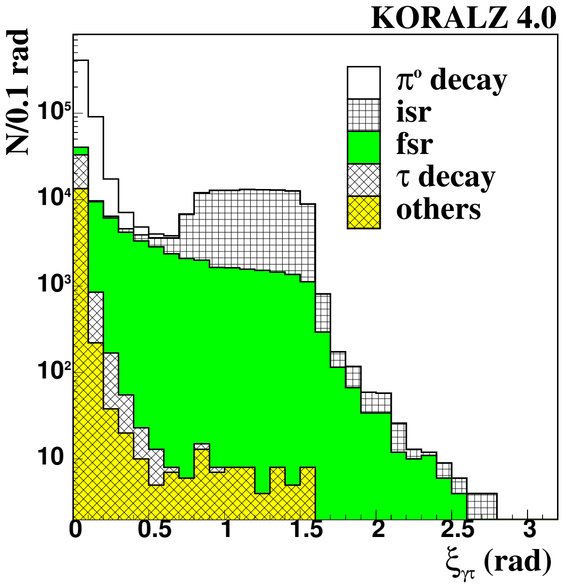

Figure 8. Isolation angle distribution of photon candidates prior to the energy and isolation cuts, for the KORALZ simulated event sample.

Figure 9 shows the energy spectrum of photons for data (points with error bars) and the results of the fit (full histogram) which is completely dominated by standard model initial and final state radiation. The shaded histogram corresponds to photons from π^0 decays. The result of the fit is

$$F_2^2(q^2 = 0) = -0.0028 \pm 0.0020^{+0.0010}_{-0.0007} \qquad (7)$$

where the first error is statistical and the second error is systematic. The systematic error is dominated by efficiency uncertainties and the limited statistics of the Monte Carlo samples used to estimate the background. Since this result is consistent with zero we convert it to an upper limit on $F_2(0)^2$ of

$$F_2^2(q^2 = 0) < 0.0024 \qquad (8)$$

at the 90% confidence level, where the non-physical region $F_2^2(0) < 0$ is excluded. This limit corresponds to $F_2(0) < 0.049$, although it should be emphasised that naively taking the square-root does not preserve the 90% confidence level meaning of this number.

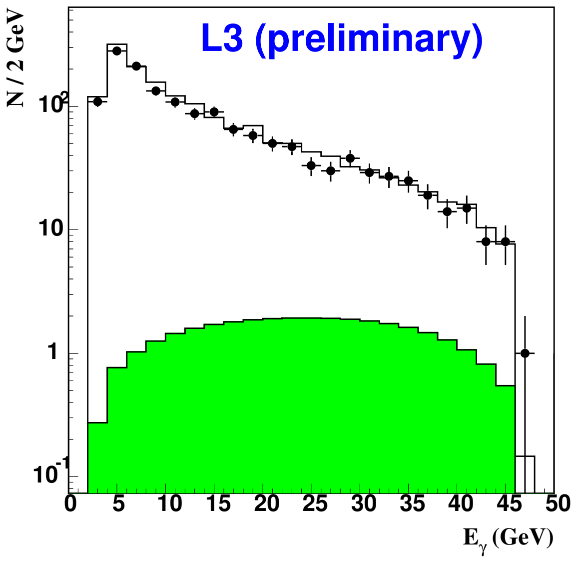

Figure 9. Energy spectrum after application of all cuts. The data are denoted by points with error bars. The full histogram shows the result of the fit, the shaded portion of which corresponds to photons from π^0 decays.

To obtain constraints on the electric dipole moment form factor, $F_3^2(q^2 = 0)$, the substitution $F_2(e/2m_\tau) \longrightarrow eF_3$ is made yielding:

$$\left(eF_3(q^2 = 0)\right)^2 < \left(2.7 \times 10^{-16} e\,\mathrm{cm}\right)^2 \qquad (9)$$

at the 90% confidence level. Again, we emphasise that the square root of this quantity does not yield a 90% confidence level constraint on $eF_3(q^2 = 0)$. These results are both consistent with the standard model.

4. DISCUSSION

4.1. Theoretical predictions

The theoretical description of the effects of anomalous moments has several weaknesses. It only makes predictions for the energy spectrum of photons. From a practical standpoint, it would be preferable to have a full prediction of the 4-vectors of all final state particles. This would allow events to be passed through the detector simulation and event reconstruction programs, yielding a more complete treatment and understanding of the acceptance and selection cuts. From a conceptual standpoint it would be preferable to include all contributing Feynman diagrams in the matrix element computation, *i.e.* standard model initial state radiation, final state radiation (with standard model and anomalous contributions), both photon and Z exchange, and all interference terms.

To address these issues, we have recently performed the full tree-level calculation without making any approximations and without neglecting any terms[11]. The resulting generator program yields 4-vectors for the final state taus and photon which can be interfaced with KORALZ to perform the decays of the taus. Preliminary studies show that the terms linear in F are not identically zero, as might reasonably be suspected, since the radiating tau is not on mass-shell. Moreover, these terms dominate over the F^2 terms in the region of the experimental sensitivity. For example, for $F = 0.01$, inclusion of the linear terms enhances the number of excess photons, compared to the purely quadratic calculation, by a factor of approximately five.

4.2. Derivation of limits

In calculating the limits quoted we implicitly assume that the Bayesian prior probability distribution is flat in F_2^2, which is proportional to the number of excess events, rather than flat in F_2. Also, the region $F_2^2 < 0$ is excluded. Both these conditions tend to err on the conservative side. Since we ultimately wish to constrain F_2 this situation is not ideal. The importance of the terms linear in F_2 will solve this problem, since then the likelihood can naturally be mapped as a function of F_2 from the outset. Rather than perform a naive conversion of constraints on F_2 into constraints on F_3 the fit should be performed in two dimensions. This may also allow the effects of F_2 and F_3 to be distinguished.

4.3. Interpretation of form factors

In this paper constraints on the form factors $F_2^2(q^2 = 0)$ and $F_3^2(q^2 = 0)$ have been determined. It is commonly assumed that these correspond to the static anomalous magnetic moment (*i.e.* $F_2(q^2 = 0) \equiv a_\tau$) and the static electric dipole moment (*i.e.* $F_3(q^2 = 0) \equiv d_\tau/q_\tau$), since the radiated photon has zero q^2. This condition is necessary but not sufficient – the tau must also be on-shell on both sides of the $\tau\tau\gamma$ vertex which is only reasonable for $E_\gamma \to 0$ (as is the case for the electron and muon measurements shown in tables 1 and 2).

Table 1
Theoretical predictions and experimental measurements of the anomalous magnetic dipole moments of charged leptons.

a_e^{SM}	$= 0.001\,159\,652\,46(15)$	[12]
a_e^{expt}	$= 0.001\,159\,652\,193(10)$	[1]
a_μ^{SM}	$= 0.001\,165\,920\,2(20)$	[13]
a_μ^{expt}	$= 0.001\,165\,923\,0(84)$	[1]
a_τ^{SM}	$= 0.001\,177\,3(3)$	[3]
a_τ^{expt}	< 0.02	[14]
	< 0.01	[15]
	< 0.11	[16]
	< 0.049	L3

Table 2
Experimental measurements of the electric dipole moments of charged leptons. Theoretically, $d_\ell \neq 0$ is forbidden by both T and P invariance.

d_e^{expt}	$= (-2.7 \pm 8.3) \cdot 10^{-27}\, e\,\mathrm{cm}$	[17]
d_μ^{expt}	$= (3.7 \pm 3.4) \cdot 10^{-19}\, e\,\mathrm{cm}$	[18]
d_τ^{expt}	$< 1.4 \cdot 10^{-16}\, e\,\mathrm{cm}$	[19]
	$< 0.5 \cdot 10^{-16}\, e\,\mathrm{cm}$	[15]
	$< 6.0 \cdot 10^{-16}\, e\,\mathrm{cm}$	[16]
	$< 2.7 \cdot 10^{-16}\, e\,\mathrm{cm}$	L3

Even the $q^2 = 0$ condition is not satisfied for the published tau measurements shown in tables 1 and 2 since these constraints are derived from analyses of the production rates and/or angular distributions of $e^+e^- \rightarrow \tau^+\tau^-$ events, in which the tau couples to the off-shell photon propagator. We therefore urge caution in the interpretation of the limits obtained on the form factors F_2 and F_3 in terms of the static tau properties, a_τ and d_τ.

REFERENCES

1. E. R. Cohen and B. N. Taylor. *Rev. Mod. Phys.*, 59:1121, 1987.
2. W. J. Marciano. 1990. Proceedings of the BNL Summer Study on CP Violation, Brookhaven National Laboratory, eds. S. Dawson and A. Soni.
3. G. Li M. A. Samuel and R. Mendel. *Phys. Rev. Lett.*, 67:668, 1991.
4. B. Adeva *et al.*L3 Collab. The construction of the l3 experiment. A 289:35, 1990.
5. O. Adriani *et al.*L3 Collab. Results from the l3 experiment at lep. *Physics Reports*, 236(CERN-PPE/93-31):1, 1993.
6. B.F.L. Ward S. Jadach and Z. Wąs. 66:276, 1991.
7. S. Jadach, J.H. Kühn and Z. Wąs. *Comp. Phys. Comm.*, 64:275, 1991.
8. E. Barberio, B. van Eijk and Z. Wąs. *Comp. Phys. Comm.*, 66:128, 1991.
9. The L3 detector simulation is based on GEANT Version 3.15.
   See R. Brun *et al.*, "GEANT 3", CERN DD/EE/84-1 (Revised), September 1987.
   The GHEISHA program (H. Fesefeldt, RWTH Aachen Report PITHA 85/02 (1985)) is used to simulate hadronic interactions.
10. D. Bardin *et al.*, FORTRAN package ZFITTER, and preprint CERN–TH. 6443/92;
    D. Bardin *et al.*, Z. Phys. **C 44** (1989) 493;
    D. Bardin *et al.*, Nucl. Phys. **B 351** (1991) 1;
    D. Bardin *et al.*, Phys. Lett. **B 255** (1991) 290.
11. J. Swain S. S. Gau, T. Paul and L. Taylor. Paper in preparation.
12. T. Kinoshita and W. B. Lindquist. *Phys. Rev. Lett.*, 47:1573, 1981.
13. V. W. Hughes and T. Kinoshita. *Comm. Nucl. and Part. Phys.*, 14:341, 1985.
14. D. J. Silverman and G. L. Shaw. *Phys. Rev.*, D27:1196, 1983.
15. R. Escribano and E. Massó. *Phys. Lett.*, B301:419, 1993.
16. J. A. Grifols and A. Méndez. *Phys. Lett.*, B255:611, 1991.
17. K. Abdullah et al. *Phys. Rev. Lett.*, 65:2347, 1990.
18. J. Bailey et al. *Journ. Phys.*, G4:345, 1978.
19. F. del Aguia and M. Sher. *Phys. Lett.*, B252:116, 1990.